RSC Advances

ROYAL SOCIETY OF CHEMISTRY

www.rsc.org/advances

Zero-valent iron impregnated cellulose acetate mixed matrix membranes for the treatment of textile industry effluent

R. Saranya[a], G. Arthanareeswaran[a*], A. F. Ismail[b*], Dionysios D. Dionysiou[c], Diby Paul[d]

[a]*Membrane Research Laboratory, Department of Chemical Engineering, National Institute of Technology, Tiruchirappalli 620015, India.*

[b]*Advanced Membrane Technology Research Centre (AMTEC), Universiti Teknologi Malaysia, 81310 UTM, Skudai, Johor, Malaysia*

[c]*Environmental Engineering and Science Program, Department of Biomedical, Chemical and Environmental Engineering (DBCEE), 705 Engineering Research Center, University of Cincinnati, Cincinnati, OH 45221-0012*

[d]*Department of Environmental Engineering, Konkuk Univeristy, Seoul, Republic of Korea*

*Corresponding author Tel +91431-2503118; Fax +91431-2500133

Email address: arthanaree10@yahoo.com (G. Arthanareeswaran), afauzi@utm.my (A.F. Ismail)

Abstract:

Novel green synthesized zero valent iron (ZVI) nanoparticles of distinct mass fractions of 0.5, 1.5 and 2.5 wt. % are blended with cellulose acetate (CA) to prepare CA/ZVI mixed matrix membranes (MMMs). The thermal stability and roughness have been improved upon increasing the mass fraction of ZVI in CA. The morphology of prepared CA/ZVI membranes has been studied using transmission scanning electron microscopy (TEM). Pure water permeability (PWP) is increased while adding 0.5 wt. % of ZVI nanoparticles. When 2.5 wt. % is added, PWP decreased due to aggregation of ZVI nanoparticles in CA polymer matrix. The adsorption capacity of ZVI nanoparticles on CA/ZVI membrane during polymer enhanced ultrafiltration of textile effluent is also investigated. The equilibrium adsorption isotherms are well fitted with Freundlich model implying the influence of active adsorptive sites of ZVI nanoparticles.

Keywords: zero valent iron; cellulose acetate; adsorption; polymer enhanced ultrafiltration; textile industry effluent

1. Introduction

The advent of nanotechnology has caused a tremendous attention towards modification of polymeric ultrafiltration membranes using novel nanomaterials. Among various nanomaterials, use of inorganic metal nanoparticles are been focussing in recent years[1]. Modification of membrane polymeric matrix using such metal nanoparticles is gaining prime importance in order to enhance the membrane filtration performance. Recent trends in membrane separation involve mixed matrix membranes (MMMs) as they offer plethora of advantages such as higher removal efficiency and flow rate, excellent selectivity, reusability, superior kinetics and leaves smaller footprint[2, 3]. The unique physico-chemical, mechanical and functional properties of inorganic metal nanomaterials will be combined with the easy processibility of organic polymeric membrane for synthesizing MMMs[4]. Hence, blending of such metal nanoparticles enable to develop MMMs having (i) enhanced removal efficiency of the pollutants in the wastewater stream by means of adsorption and catalytic reaction, (ii) thermal stability for operating at very high temperatures[5-7]. Since the discovery of asymmetric membranes by Leob and Sourirajan[8], cellulose acetate (CA) has been considered as an important polymeric material for its higher hydrophilicity and easy processibility. However, CA membrane having excessive fouling, lower pH and thermal stability, lesser reproducibility and so on[9, 10] necessitates modification for better performance. For modification of CA, both bulk and surface modification approaches such as blending, grafting, surface coating have been so far reported[11-13]. As the success of MMMs mostly depend on the control of interfacial defects between polymeric matrix and inorganic modifiers[14], the choice of modifiers play an important role in novel MMMs synthesis.

Zero valent iron (ZVI) nanoparticles, due to their high surface reactivity and smaller size[15] can transform complex pollutants such as polychlorinated biphenyls (PCBs),

trichloroethylene (TCE), recalcitrant dye compounds and chlorinated organic solvents[16]. The zero oxidation state of iron is termed as ZVI and it has completely filled d-orbitals thus likely to readily loose electrons making it very reactive[17]. The reactive and hydrophilic properties of ZVI nanoparticles make it best suited for polymeric membrane modification[18]. Several methods to synthesize ZVI had been carried out but the main challenges of these methods lie in their capacity to obtain a narrow dispersion of the particle without losing the desired compositional, structural and crystalline uniformity[19]. Various stabilisers have been utilised in efforts to obtain smaller, segregated and stable ZVI nanoparticles[20, 21]. The green synthesis of ZVI with the help of stabilising and reducing polyphenols especially with the use of green tea extract is thus widely under research[22, 23].

A simple approach of using green tea extract as a reducing and stabilizing agent for generating ZVI nanoparticles has been performed in this study. The alcoholic functional groups containing in tea extract is responsible for the both reduction and stabilisation of nanoparticles. The tea extract (poly phenols) thus helps in the formation of relatively stable nanocrystals ZVI so that aggregation and passivation of such nanoparticles are been avoided[24]. Moreover, polyphenols as capping agents in the ZVI particles tend to form complexes with pollutants and thus can reduce the metals and dye compounds present in the wastewater. It was widely recognized that Vander Waals and magnetic forces of ZVI particles induces them to agglomerate thus inhibiting its reactivity and mobility towards the targeted pollutants[25]. Such effect is much more intense in case of magnetite iron oxide nanoparticles when compared to ZVI. The synthesis of ZVI from polyphenols thus helps in providing strong steric hindrance due to inter-particle electrostatic interactions so as to overcome the attractive Vander Waals and magnetic forces between iron particles. Based

on all these advantages, the source for ZVI nanoparticle synthesis was identified as the reduction of ferric chloride using polyphenol extract from green tea leaves.

Many conspicuous interesting results were reported on the remarkable impact of iron based nanoparticles such as iron oxide as filler in membrane separation applications such as pervaporation of organic solvents and heavy metal remediation[26]. However, the utilisation of green synthesized ZVI nanoparticles for polymeric membrane modification to improve the efficiency of UF process in treating textile industry effluent has not been studied so far. Among several mechanisms, adsorption is the most commonly used process to remove the dye constituents of textile industry effluent. Hence, the combination of different methods like adsorption and filtration for enhanced membrane separation is highly presumed in order to achieve significant reduction on pollutants in textile industries. Adsorption is one of the most commonly used processes to remove the dye compounds from textile industry effluent. The synergistic effect of permeation and adsorption is supposed to be favoured using CA/ZVI MMM for the removal of pollutants from the textile industry effluent. Indeed, the impact of adsorption on a membrane surface in terms of improving the rejection performance is a complex phenomenon and still there remains an ambiguity thus requiring more investigation on such studies[27]. Hence, this work has attempted an insight of employing both the adsorptivity and perm-selectivity of ZVI nanoparticles during UF process. The feasibility of modifying CA membranes using green synthesized ZVI was studied initially. Further, the role of ZVI for an enhanced membrane filtration was investigated by blending with cellulose acetate (CA). The membrane characterisations in terms of pore morphology and surface topography have been studied. The reduction of chemical oxygen demand (COD), biological oxygen demand (BOD) and sulphates from textile industry effluent was quantified and compared with virgin CA membrane.

2. Experimental

Materials

All chemicals and reagents used were of analytical grade and used without any further purification. Commercial grade CA obtained from Mysore Acetate and Chemicals Co. Ltd., India was used after recrystallization from acetone. Analytical grade acetone was procured from Merck (India) Ltd. N, N'-dimethyl formamide (DMF) was purchased from Qualigens fine chemicals, Glaxo India Ltd. Green tea leaves were purchased from Tamilnadu tea (TANTEA) plantation Corporation, India. Ferric chloride was obtained from Merck (India) Ltd. Polyethyleneimine (PEI, Mw: 50 KDa) was obtained from Alfa Aesar (India) limited. The textile dye effluent was collected from the KG fabrics limited located at Erode and the physico-chemical characteristics of the collected effluent are given in Table 1.

Synthesis of ZVI Nanoparticles

ZVI nanoparticles (Fe (0)) synthesis using various conventional reducing agents like sodium borohydride has been reported in several previous studies[19, 21]. Such reducing agent employed in several of such traditional methods poses toxicity and lesser solubility imparting high temperature and pressure conditions for the ZVI synthesis. Plant based reducing agents such as polyphenols from grapes, coffee and so on have also been employed for nanoparticle synthesis however gets oxidized slowly[17]. In the present study, green tea extract being non-toxic and highly water soluble is been considered as the environmental friendly reducing polyphenol. In addition, green tea extract constitutes the highest % of polyphenol which will be suitable for yielding ZVI nanoparticles. The reaction of ferric chloride ($FeCl_3$) with green tea extract as the reducing polyphenol formed the basis for the green synthesis of ZVI nanoparticles. 20 g/L of green tea leaves were

brewed at the temperature of 80º C later which was later vacuum filtered to obtain the green tea extract. The synthesis and the impregnation of ZVI on CA matrix have been illustrated in Fig. 1. The synthesis procedure follows the bottom-up approach by which $FeCl_3$ gets reduced by green tea extract even in room temperature. 0.5 M $FeCl_3$ and prepared green tea extract was mixed in the ratio of 2:1 and kept under stirring at 250 rpm in ambient conditions to prepare ZVI solution. The solution was then centrifuged for 10 min at 6000 rpm to obtain the pellet. The resultant pellet has been washed twice with deionised water and vacuum dried for 24 h at 105º C to obtain ZVI nanoparticles.

Characterisation of ZVI Nanoparticles

The synthesized ZVI nanoparticles were then characterised for its particle size using particle size analyser (Nanopartica, Hiroba, USA). The zeta potential of ZVI nanoparticle was also determined using zetasizer (Malvern). The crystallite phase of ZVI has also been studied by means of X-ray diffractogram (XRD, Rigaku Corporation, Japan). The crystallite size (D) of ZVI has been found with the help of Scherrer Eq. (1):

$$D = \frac{0.9\lambda}{\beta \cos \vartheta} \quad (1)$$

where λ is the X-ray wavelength and β is the full-width half maximum (FWHM) of the intensity peak. The morphology of synthesized ZVI was also visualised using the transmission electron microscopy (FEI Technai F20 S, USA) and the elemental analysis has been performed by energy dispersive X-ray analysis (EDAX) to confirm the elemental form of ZVI nanoparticles.

Preparation of CA/ZVI MMMs

The phase inversion method was employed for fabrication of CA/ZVI MMMs. Different CA casting solutions were prepared by adding 0.5, 1.5 and 2.5 wt. % of ZVI

nanoparticles each with CA. The compositions of casting solutions are provided in Table 2. The homogenous casting solution for each composition was obtained by dispersing ZVI initially in DMF solvent which after complete dissolution by means of ultrasonication was mixed with CA under mechanical stirring. The final mixture was also sonicated for 30 min before casting to ensure homogeneity and then cast for the thickness of 400 µm using a film applicator (Elicometer (Asia) Ltd, Singapore) on a glass plate. After allowing for 30 s evaporation time, the cast membrane was immersed in distilled water maintained at 20° C. The prepared CA/ZVI MMMs were then preserved in 1 % formalin added distilled water to prevent them from microbial and other contamination.

Thermal Properties of CA/ZVI MMMs

Thermal stability of CA and CA/ZVI membranes were analysed by thermal gravimetric analysis (TGA) coupled with differential scanning calorimetry (DSC) using thermal analyser (TA, Model SDT 2000, USA). The membrane samples initially dried in vacuum oven at 180° C were analysed between the temperature range of 10° to 600° C with 10° C/min heating rate under nitrogen gas supply. The thermal decomposition temperature (T_d) is the starting temperature at which the decomposition of membrane sample initiates. Hence T_d and the wt. % loss on corresponding T_d can be calculated from each thermogram to investigate the effect of ZVI addition in increasing the onset of T_d. The glass transition temperature (T_g) was also determined to know the ZVI influence in improving the heat withstanding ability of CA/ZVI MMMs.

Surface Roughness Analysis of CA/ZVI MMMs

The surface characterisation of CA/ZVI membranes was performed using atomic force microscopy (NT-MDT modular AFM, NTEGRA Prima, Ireland). High resolution

two and three dimensional surface images were taken for the comparison of surface roughness between CA and CA/ZVI MMMs. With the help of Nova-NTEGRA AFM software, the images were processed with a sample scan area of 30 μm x 30 μm for measuring average roughness and root-mean-squared roughness (R_{rms}) values for each membrane. As there is a linear relationship between membrane permeability and roughness[28], the measure of roughness helps to know the extent of hydrophilicity of the synthesized CA/ZVI membranes which could in turn be related to the permeability.

Morphological Characterisation of CA/ZVI MMMs

The top and cross-section morphology of synthesized membranes were visualized with the help of field emission scanning electron microscopy (FESEM, Hitachi, S-4160, Japan) operated at an accelerating voltage of 20 kV. The dried membrane samples were pre-treated using gold (Au) sputtering to impart electrical conductivity. The variation in pore morphology between CA and CA/ZVI MMMs were visualised based on this study.

Ultrafiltration Performance of CA/ZVI MMMs

Pure Water Flux Studies

The permeability of CA and CA/ZVI MMMs were compared by measuring the pure water flux with the help of dead-end stirred cell (model Cell-XFUF076, Millipore, USA) UF unit. Experiments was performed at 414 kPa trans-membrane pressure (TMP) and 500 rpm stirring speed by mounting the synthesized membranes on a stirred cell UF unit. The permeate volume was collected every 10 min until reaching steady state for which the pure water flux (J_{w1}) was calculated using the following Eq. (2):

$$J_{w1} = \frac{V}{A \times \Delta t} \quad (2)$$

where V, A and Δt are the permeate volume, membrane effective area and permeation time respectively.

Treatment of Textile Industry Effluent

The rejection performance of each CA/ZVI MMMs was quantified by performing treatment of textile industry effluent in dead-end stirred cell to evaluate the reduction of COD, BOD and $SO4^{2-}$. The reduction of COD and other characteristics from textile effluent will be still more efficient by complexing the effluent with PEI, water-soluble macroligands[29]. The concentration of water-soluble macroligands PEI was maintained at 1 wt. %. To achieve complete binding, PEI and textile dye effluent was mixed thoroughly under vigorous stirring for 24 h[30].

Under the TMP of 414 KPa, the textile effluent has been treated using CA and CA-ZVI-1 MMM. The permeate has been collected periodically at an interval of 10 mins for 120 mins of filtration. The effluent flux recorded at the end of 120 mins has been labeled as J_{eff}. The membrane was then washed to remove the fouling layer and PWP was again measured as J_{w2}. The PEI complexed textile effluent was then passed through CA and CA/ZVI-1 MMM for the period of 120 mins to record the flux as $J_{PEI\text{-}eff}$. Finally, with the help of deionized water PWP flux was again measured and noted as J_{w3}. The collected permeate volume from effluent and PEI bound effluent has been analysed for COD, BOD and SO_4^{2-} using the standard methods[31]. As fouling recovery rate (FRR) % enables to determine the extent of fouling due to effluent filtration, the following Eq. (3) and (4) has been followed to determine FRR % after effluent and PEI-bound effluent treatment.

$$FRR_{eff}(\%) = \frac{J_{w2}}{J_{w1}} \times 100 \quad (3)$$

$$FRR_{PEI\text{-}eff}(\%) = \frac{J_{w3}}{J_{w1}} \times 100 \quad (4)$$

The rejection efficiency of CA/ZVI-1 MMM on removal of COD, BOD and SO_4^{2-} due to PEI complexation was determined using the Eq. (5):

$$\%\text{Rejection} = 1 - \frac{C_p}{C_f} \times 100 \quad (5)$$

Where C_p and C_f are the concentration of permeate and feed respectively.

The adsorption taking place in CA/ZVI-1 membrane was also examined by quantifying the equilibrium concentration (mg/L) of COD, BOD and SO_4^{2-} remaining after UF experiment. The PEI bound effluent sample of volume (V) 100 ml was taken as feed and the adsorption capacity (Q_e) was determined at various time intervals. The effective membrane area (A) in contact with the solution was 38.5 cm^2. During the adsorption enhanced batch filtration, natural pH of the effluent was maintained which was about 5.5. The extent of adsorption on CA/ZVI-1 membrane during polymer enhanced UF of PEI bound textile industry effluent was also investigated using the following Eq. (6):

$$Q_e = \frac{(C_b - C_{eq})}{A} \times V \quad (6)$$

where C_b and C_{eq} are the blank and equilibrium concentrations of COD. BOD and SO_4^{2-} for measuring the COD, BOD and SO_4^{2-} adsorption on CA/ZVI-1 MMM.

3. Results and Discussion

Size and Crystallite Analysis of ZVI Nanoparticles

The crystallite size of the ZVI nanoparticles was found to be as 27.8 nm from the XRD profile as shown in Fig. 2 using Eq. (1). The intensity peaks at 28.75°, 39.5º are found to have miller indices of (110) and (211) which are matching with standard (JCPDS

75-0033) characteristics of zero valent iron (Fe (0)). The typical ZVI exhibits core-shell structure core consisting of core metallic iron whereas the oxide shell constitutes Fe^{2+} and Fe^{3+} as a result of atmospheric oxidation[21]. The peak at 45.76° corresponds to (300) suggesting the occurrence of ferrihydrite (FeOOH) in ZVI nanoparticles[32]. The nanoparticle size of 32.5 nm with the higher particle size distribution of 25 to 35 nm has been observed as shown in Fig. 3 and surface area of ZVI 28.2 m^2/g as found by particle size analyser also has confirmed the nanoscale of synthesized ZVI particles and hence its higher reactivity on impregnating it into CA matrix.

Morphology and Zeta Potential of ZVI Nanoparticles

The morphology of synthesized ZVI nanoparticles as shown in Fig. 4 is appeared to be in clear crystal structure formation and tended to aggregate distinctly with a particle size of about 25 to 35 nm. Some of the particles are also found to be placed without aggregation due to steric hindrance and such forces help for intense dispersion of ZVI nanoparticles in CA matrix. The spectral measurements were also recorded that indicated the EDAX spectra showing the metallic form of Fe as in Fig. 5. Further, the stability of ZVI nanoparticles has been confirmed by the zeta potential measurement as shown in Fig.6. The higher zeta potential of about -24.5 mV of ZVI nanoparticles also implies its higher stability. The negative zeta potential of ZVI nanoparticles of more than 20 mV reassures the presence of large number of negative charge on its surface and its stability[33]. This ultimately helps in achieving homogenous CA/ZVI cast solution at minimal loading of ZVI nanoparticles.

Thermal Behaviour of CA/ZVI MMMs

The thermal properties of CA and CA/ZVI membranes in terms of T_d, wt. % loss and T_g are shown in Table 3. The T_d value was higher for all CA/ZVI MMMs when

compared to the value of 247.8° C of CA membrane. The superior interaction of ZVI with CA has loosened the segmental mobility of CA[34] thus offering higher thermal stability to CA/ZVI membranes. The highest T_d value of 315.76° C was observed when 2.5 wt. % ZVI particles were added in CA polymer matrix (CA/ZVI-3 MMM). The increase in ZVI content has also caused the prominent shielding effect on CA and hence the thermal stability has also increased for CA/ZVI-3 membrane. The thermal profile shown in Fig. 7 also depicts the reduction in wt. % loss during decomposition for ZVI added membranes. The high interfacial mixing of inorganic ZVI and organic CA lead to the pronounced effect of thermal stability depicted by increase in T_d and reduction in decomposition loss. The derivative weight loss was lesser of about 34.27 % for 2.5 wt. % containing ZVI nanoparticles. This has further implied that the increased loading of ZVI has rendered reduction of residual weight % to CA/ZVI-3 MMM as shown in Table 3.

The transition temperature found from DSC curve (Fig. 8) as indicated in Table 3 also increased from 191.2º C to 201.5º C, implying the improvement in thermal stability of ZVI incorporated MMMs in comparison with CA. The highest T_g of 218.4° C was obtained for 2.5 wt. % containing CA/ZVI-3 MMM (Fig. 8). The higher onset of T_g in CA/ZVI-3 membrane denotes good adhesion between ZVI and CA which weakened the interactions between CA segments. This phenomenon also indicates that the surface modification of CA has influenced the improvement in its thermal properties. The increase of T_g is owing to ZVI that restricts the movement of the polymeric chains of CA thus confirming the interaction of ZVI nanoparticles and CA.

Roughness Characteristics of CA/ZVI MMMs

The roughness characteristics (Average roughness, R_{ms} roughness) were compared based on the surface topography obtained for CA and CA/ZVI membranes. The virgin CA

indicated lower average roughness of 16.15 nm and R_{ms} roughness of 21.55 nm. The highest peaks (brightest points) and lowest valleys (darkest points) are seen in CA/ZVI-1 and CA/ZVI-2 MMM which confirmed the increase in roughness due to ZVI impregnation as shown in Fig. 9. However, higher ZVI content of 2.5 wt. % in CA/ZVI-3 membrane showed higher average roughness value of 95.32 nm and R_{ms} roughness of 123.65 nm as shown in Table 3. The reason is attributed to the increase in heterogeneity and viscosity of casting solution due to higher ZVI loadings[35]. The accumulation and lesser dispersion of ZVI nanoparticles make the delayed demixing phase inversion process that offered denser surface for CA/ZVI-3 MMM[36]. The surface roughness of CA/ZVI-3 membrane was higher compared to CA/ZVI-1 and CA/ZVI-2 membrane insisting the decrease in hydrophilicity during higher addition of ZVI nanoparticles.

FESEM Morphology of CA/ZVI MMMs

The top surface morphology of CA/ZVI membranes (Fig. 8) reveals that the ultrasonication has its significance on dispersing the ZVI nanoparticles in uniform manner in the CA matrix. From Fig. 10 (a), it can be seen that most ZVI nanoparticles were distributed uniformly on CA as shown in CA/ZVI-1 MMM. The formation of pores were largely formed on the surface of CA/ZVI-1 membranes was because of ZVI nanoparticles dragging out from the CA polymeric matrix during phase inversion. The cross-section FESEM images of CA/ZVI membrane (Fig. 10 (b)) helps to visualise the pore morphology which could be clearly related with its permeability characteristics. The dense uniform morphological structure was observed for virgin CA membrane with no differentiation of top dense and bottom porous layer. The addition of nanoparticles tends to progress the sub-layer macro-voidal formation[37] and it was highly evident in CA/ZVI-1 MMM. However, during highest ZVI loading, the nanoparticles completely loss structure thus bringing

deformation of the skin layer and pore structure[38]. This effect along with the surface pore blockage on highest addition of ZVI nanoparticles (2.5 wt. %) has caused the lesser permeability to CA/ZVI-3 when compared to CA/ZVI-1 MMM.

Effect of ZVI Nanoparticles on Permeability of CA/ZVI Membranes

The change in pure water permeability (PWP) due to the addition of ZVI has been indicated in Table 3. The addition of 0.5 wt. % of ZVI nanoparticles has improved the PWP of CA/ZVI-1 membrane. However, the increase in addition of ZVI from 0.5 wt% to 1.5 wt% has reduced the PWP from 37.17 L m^{-2} h^{-1} to 25.63 L m^{-2} h^{-1}. The permeation capacity majorly depends on the thinner top-layer of the CA/ZVI membrane and hence the increase in thickness due to increased ZVI content. The higher amount of metallic ZVI nanoparticles are found to be non-porous and the tighter aggregates of ZVI nanoparticles would lead to surface pore blockage rather than void formation as observed in CA/ZVI-1 membranes. Also, the higher loading of ZVI nanoparticles has obstructed majority of surface pores and passages[39] thus reducing the permeability. Further, the increase of ZVI nanoparticles created accumulated mass over the surface pores of CA/ZVI-3 MMM as observed in FESEM image (Fig. 8 CA/ZVI (b)). Hence, it was confirmed that there has not been any aggregation on the top layer till adding 0.5 wt. % of ZVI nanoparticles to CA. Thus minimal loading of ZVI nanoparticles helped for higher preferential flow that ultimately enhanced the permeability properties of CA/ZVI-1 membrane.

Treatment of Textile Industry Effluent

Permeability and Anti-fouling Performance of CA/ZVI MMM

In this study, the permeate flux achieved during filtration of textile effluent has been compared between CA and CA/ZVI MMM. The flux decline with respect to time as shown in Fig.11 indicates that at initial stages of treating textile effluent for CA/ZVI-1

MMM effluent flux has decreased rapidly compared to CA and reached 17.3 $Lm^{-2}h^{-1}$. The permeate flux of PEI bound effluent has been decreased to about 23.7 %. The polymer enhanced filtration by employing CA membrane has shown the permeate flux of 5.8 $Lm^{-2}h^{-1}$ which is 46.8 % lower compared to effluent treated without PEI complexation. This suggests that foulants has been deposited reversibly on the CA/ZVI-1 membrane surface as a cake layer which can be restorable by backwashing.

Comparing the FRR_{eff} and $FRR_{PEI\text{-}eff}$ value of 72 and 67.5 %, it could be deduced that flux recovery has been almost similar for both PEI bound and raw textile effluent. However, in case of CA membrane, the $FRR_{PEI\text{-}eff}$ % of 21.2 has been observed which is lesser than FRR_{eff} value of 48.7 %. This signifies that the PEI binding due to their negatively charge tends to indulge in electrostatic repulsions between the negatively charged pollutants present in the textile dye effluent which leads to a decrease in membrane surface fouling[40]. The effect of complexation of PEI with textile dye effluent enables on improving the fouling resistance due to its binding with the anionic pollutants and acidic dye compounds has been illustrated as shown in Fig. 12.

Effect of PEI Binding on Rejection Efficiency of CA/ZVI MMM

The rejection efficiency of CA/ZVI-1 membrane was investigated using textile dye effluent with and without PEI binding. The amine groups in PEI interacted with textile dye molecules that caused increase in retention of PEI bound textile dye complex effluent.

The highest BOD removal of about 95.8 % reduction was observed for PEI bound effluent owing to the presence of ZVI nanoparticles that offered biofouling resistance to CA/ZVI-1 membrane. The hydrophilic property has been exerted by the hydroxide form of iron present in the outer shell of ZVI nanoparticles[41]. The BOD concentration of retentate also gets reduced to 84 mg/l which would be due to higher adsorption by ZVI

nanoparticles present in CA. Similarly, the rejection efficiency of CA/ZVI-1 membrane in removal of COD was higher of about 90.2 % with the retentate concentration of 654 mg/l. The adsorptive property of ZVI nanoparticles has caused the reduction in retentate concentration which has been supported by the earlier works[42, 43].

In contrast to BOD and COD rejection efficiency, the SO_4^{2-} rejection of only 55.5 % was observed for CA/ZVI MMM as shown in Table 4 for PEI bound textile dye effluent. The reason for lesser SO_4^{2-} rejection is attributed to the fact that the dissolved salts pass through pores of UF membranes easily resulting in only less % rejection in comparison with that of COD and BOD. However, the reason for the higher rejection efficiency in comparison to CA membrane is attributed to the presence of Fe^{2+} cations formed in the acidic medium of the effluent owing to the presence of ZVI nanoparticles. It facilitates the active removal of divalent anions like SO_4^{2-} present in the effluent.

Effect of Adsorption during Polymer Enhanced UF

Since ZVI nanoparticles has plausible effect of adsorption during membrane filtration experiments, the adsorption taking place during UF by employing CA/ZVI-1 membrane has been studied. The adsorption capacity of CA/ZVI-1 membrane was understood by means of two classical adsorption models (i) Langmuir and (ii) Freundlich isotherms were employed to study the adsorption kinetics of the COD, BOD and SO_4^{2-} from the textile dye effluent. The Langmuir adsorption is a simple two parameters model based on the assumption that there exists a homogenous monolayer adsorption without any interaction among adsorbed pollutants[44] and can be expressed as Eq. (7):

$$Q_e = a.\frac{bC_e}{1+bC_e} \quad (7)$$

where C_e (mg/l) and Q_e are the adsorbed pollutant concentration (COD/BOD/SO_4^{2-}) and adsorption capacity respectively at equilibrium. a and b are the Langmuir adsorption constants at equilibrium.

If the adsorption over the CA/ZVI-1 membrane is assumed to be heterogenous with the assumption that adsorption energy of adsorbed species depends on the availability of the adjacent active unoccupied adsorbent site of ZVI nanoparticles[45], Freundlich isotherm model is considered as following Eq. (8):

$$Q_e = b.C_e^{\ m} \tag{8}$$

where *b* and *m* represents Freundlich isotherm constants in which *m* indicates intensity and favorability of adsorption. The lower value of *m* and higher value of *b* suggests stronger reaction of ZVI nanoparticles towards pollutant species and hence increased removal respectively[46].

The plot between Q_e, (the amount of pollutants (COD, BOD and SO_4^{2-}) adsorbed) and C_e, (the equilibrium concentration of pollutants remaining (mg/L)) were found to indicate the higher R^2 value (~ 0.9957) and fitting for Freundlich isotherm as compared to Langmuir having the R^2 value (~ 0.8578). The well representation of Freundlich isothermal constants would also help to understand that the favourable adsorption of COD, BOD and SO_4^{2-} over CA/ZVI-1 membrane.

Effect of Adsorption and PEI Binding on Rejection Efficiency of CA/ZVI MMM

To determine the influence of adsorption in improving the rejection efficiency of CA/ZVI-1 MMM, the experimental adsorption capacity has been correlated with the adsorption isotherms. The adsorption constants determined owing to the adsorption of textile dye effluent with and without PEI are shown in Table 5.

The binding of PEI enhanced the both the adsorption and rejection efficiency as the value of '*m*' comes down from 0.49 to 0.39 for BOD adsorption thus favouring the adsorption of PEI bound pollutants on CA/ZVI-1 membranes. This is due to the interaction of –NH in PEI with the electrons of ZVI thus helping to improve the efficient adsorption of COD and BOD exhibiting pollutants on the surface of CA/ZVI-1 membrane. The presence of ZVI nanoparticles has helped potentially for the adsorption of PEI complexed pollutants due to its surface acidity that tends involve in proton exchange. Therefore, the experimental R^2 fitting for adsorption of PEI bound effluent has higher value of 0.9957 than effluent without PEI binding showing R^2 0.9852 during polymer enhanced UF (Fig. 13).

The higher colloidal stability of synthesized ZVI nanoparticles helps to retain the active adsorptive sites without aggregation thus increasing the adsorption affinity[47]. The efficient dispersion and higher stability of ZVI nanoparticles would strongly influence the accessibility of its adsorption sites[48]. The affinity of surface oxygen and reactive property of ZVI also helped for greater adsorption of organic compounds thus resulting in favourability of reduction of BOD and COD. The nano-sized ZVI has the reactivity and reducing ability and hence the COD exhibiting pollutants present in the textile effluent could be easily reduced. The similar trend of reduction in *m* value as shown in Table 5 helped to infer the benefit of PEI complexation along with membrane adsorption for COD and SO_4^{2-} reduction. The adsorption isotherm of COD and SO_4^{2-} on CA/ZVI-1 membrane is depicted in Figs. 14 and 15 respectively.

The isothermal constant *m* has also been decreasing owing to PEI binding thus suggesting the increase in adsorption capacity of CA/ZVI-1 membrane even for PEI bound effluent. Moreover, the high specific surface area of ZVI nanoparticles tends to have relatively higher affinity towards inorganic oxoanions like SO_4^{2-}. Hence, SO_4^{2-} molecules

were known to be exchanged for its divalent ferrous cations (Fe^{2+}) of ZVI nanoparticles thus showing comparable rejection of SO_4^{2-} from the textile industry effluent.

4. Conclusions

The greener method of ZVI nanoparticle synthesis was carried out in this study. The influence of ZVI nanoparticles in altering the entire pore structure and morphology of CA/ZVI MMMs was investigated. The intrinsic properties of ZVI nanoparticles enabled the increase in thermal stability and surface roughness of CA/ZVI membranes. Adsorption capacity of ZVI nanoparticles and PEI binding has influenced the rejection efficiency of CA/ZVI membrane thus reaching highest BOD, COD and SO_4^{2-} removal of about 96.7%, 90.2% and 55.5% respectively. The adsorption isothermal study of CA/ZVI-1 membrane showed efficient adsorption removal for PEI binding effluent and the experimental values correlated well with Freundlich isotherm model. The enhancement of rejection performance by means of adsorptive nanoparticles would have remarkable effect on the importance of nanostructured modification of polymeric membrane.

References

1. M.M. Pendergast and E.V.M. Hoek, *Energy Environ. Sci.,* 2011, 4, 1946.
2. A. Ghaee, M. Shariaty-Niassar, J. Barzin and T. Matsuura, *Chem. Eng. J.,* 2010, 165, 46.
3. R. S. Vieira, E. Guibal, E. A. Silva and M. M. Beppu, *Adsorption*, 2007, 13, 603.
4. Y. L. Thuyavan, N. Anantharaman and G. Arthanareeswaran, *Ind. Eng. Chem. Res.,* 2014, 53, 11355.

5. P.K. Stoimenov, R.L. Klinger, G.L. Marchin and K.J. Klabunde, *Langmuir*, 2002, 18, 6679.
6. N. Savage and M.S. Diallo, *J. Nanopart. Res*., 2005, 7, 331.
7. Y.C. Sharma, V. Srivastava, V.K. Singh, S.N. Kaul and C.H. Weng, *Environ. Technol.*, 2009, 30, 583.
8. S. Loeb and S. Sourirajan, *Adv. Chem. Ser*., 1963, 38, 117-132.
9. G. Arthanareeswaran, D. Mohan and M. Raajenthiren, *App. Surf. Sci*., 2007, 253, 8705.
10. E. Ostuni, R.G. Chapman, R.E. Holmlin, S. Takayama and G.M. Whitesides, *Langmuir* 2001, 17, 5605.
11. A. Jayalakshmi, S. Rajesh and D. Mohan, *App. Surf. Sci*., 2012, 258, 9770.
12. S. Rajesh, K.H. Shobana, S. Anitharaj and D.R. Mohan, *Ind. Eng. Chem. Res.*, 2011, 50, 5550.
13. W. Zhou, J. He, S. Du, S. Cui and W. Gao, *Iran. Poly. J*., 2011, 20 (5), 389.
14. Y. Shen and A. C. Lua, *Chem. Eng. J.*, 2012, 192, 201.
15. X.Q. Li, D. Brown and W.X. Zhang, *J. Nanopart. Res*., 2007, 9, 233.
16. J. Xu, A. Dozier and D. Bhattacharyya, *J. Nanopart. Res.,* 2005, 7(4–5), 449.
17. C. Chrysochoou, G. Johnston and G. Dahal, *J. Haz. Mater.*, 2012, 201-202, 33.
18. I. Martinez-Mera, M.E. Espinosa-Pesqueira, R. Perez-Hernandez, R and J. Arenas-Alatorre, *Mater. Lett*., 2007, 61, 4447.
19. V. Smuleac, L. Bachas and D. Bhattacharyya, *J. Membr. Sci.*, 2010, 346(2), 310.
20. S. Lewis, A. Lynch, L. Bachas, S. Hampson, L. Ormsbee and D. Bhattacharyya, *Environ. Eng. Sci.*, 2009, 26 (4), 849.
21. G.E. Hoag, J.B. Collins, J.L. Holcomb, J.R. Hoag, M.N. Nadagoud and R.S. Varma, *J. Mater. Chem*., 2009, 19, 8671.

22. M.N. Nadagoud, A.B. Castle, R.C. Murdock, S.M. Hussain and R.S. Varma, *Green. Chem.*, 2010, 12, 114.

23. P. Prema and M. Selvarani, *Int. J. Res. Chem. Environ.*, 2012, 2 (4), 115.

24. D.V. Franco, L.M. Da Silva and W.F. Jardim, *Water, Air, and Soil Poll.,* 2009, 197, 49–60.

25. P. Daraei, S.S. Madaeni, N. Ghaemi, E. Salehi and M.A. Khadivi, *J. Membr. Sci*., 2012, 415–416, 250.

26. P. Daraei, S.S. Madaeni, N. Ghaemi, M.A. Khadivi, B. Astinchap and R. Moradian, *Sep. Purif. Technol.,* 2013, 109, 111.

27. Sotto, J.M. Arsuaga and B.V. Bruggen, *Desalination,* 2013, 309, 64.

28. M. Hirose, H. Ito and Y. Kamiyama, *J. Membr. Sci.,* 1996, 121(2), 209.

29. G. Arthanareeswaran, P. Thanikaivelan, N. Jaya, D. Mohan and M. Raajenthiren, *J. Hazard. Mater.,* B. 2007, 139, 44.

30. R.S. Juang and M.N. Chen, *Ind. Eng. Chem. Res.* 1996, 35, 1935.

31. APHA, Standard methods for the examination of water and waste water, American Public Health Association, Washington, 21st edn, 2005.

32. S. Laurent, D. Forge, M. Port, A. Roch, C. Robic, L. V. Elst and R. N. Muller, *Chem. Rev.,* 2008, 108, 2064.

33. H. Kisch, S. Sakthivel, M. Janczarek and D. Mitoraj, *J. Phy. Chem. C*., 2007, 111, 11445.

34. K. Chrissafis and D. Bikiaris, *Thermochimica. Acta.,* 2011, 523, 1.

35. F. Moghadam, M.R. Omidkhah, E. Vasheghani-Farahani, M.Z. Pedram and F. Dorosti, *Sep. Purif. Technol*., 2011, 77, 128.

36. N. Ghaemi, S.S. Madaeni, A. Alizadeh, H. Rajabi and P. Daraei, *J. Membr. Sci*., 2011, 382, 135.

37. V. Vatanpour, S.S. Madaeni, R. Moradian, S. Zinadini and B. Astinchap, *J. Membr. Sci.,* 2011, 375, 284.

38. Y. L. Thuyavan, N. Anantharaman, G. Arthanareeswaran, A. F. Ismail and R. V. Mangalaraja, *Desalination*, 2015, 365, 355.

39. A. Gholami, A.R. Moghadassi, S.M. Hosseini, S. Shabani and F. Gholami, *J. Ind. Eng. Chem*., 2014, 20 (4)*,* 1517.

40. B. I. Kharisov, H. V. Rasika Dias, O. V. Kharissova, V. M. Jimenez-Perez and B. O. Pereza, *RSC Adv.,* 2012, 2, 9325.

41. J. Alam, L.A. Dass, M. Ghasemi and M. Alhoshan, *Polym. Compos*., 2013, 34(11), 1870.

42. F. Belaib, A.H. Meniai, M. Bencheikh-Lehocine, A. Mansri, M. Morcellet, M. Bacquet and B. Martel, *Desalination*, 2004, 166, 371.

43. L.Y. Ng, A.W. Mohammad, C.P. Leo and N. Hilal, *Desalination*, 2010, 261(3)*,* 313.

44. X. Wang, L. Zhang, C. Ma, R. Song, H. Hou and D. Li, *Hydrometallurgy*, 2009, 100, 82.

45. S.S. Madaeni and E. Salehi, *J. Membr. Sci.,* 2009, 333, 100.

46. M. Ajmal, M. Ali, R. Yousuf and A. Ahmed, *Indian. J. Environ. Health.,* 1998*,* 40 (1)*,* 15.

47. S. R. Panda, M. Mukherjee and S. De, *J. Water. Process. Eng.,* 2015, 6, 93.

48. R. Saranya, M. Kumar, R. Tamilarasan, A. F. Ismail and G. Arthanareeswaran, *J. Chem. Technol. Biotechnol.,* 2015, 25, 152.

List of Tables

Table 1. Physico-chemical characteristics of textile dye effluent

S. No.	Characteristics	Value
1.	Color	Dark Brown
2.	pH	8.92
3.	Total Hardness (mg/L)	871
4.	Turbidity (NTU)	61
5.	Total dissolved solids (mg/L)	22451
6.	Conductivity (Micromho's/cm)	34258
7.	BOD_5 at 20^o C (mg/L)	364
8.	COD (mg/L)	1184
9.	Sulphates (mg/L)	2180
10.	Total Alkalinity as $CaCO_3$ (mg/L)	3854

Table 2. Casting composition of CA/ZVI MMMs

Membrane Type	Casting solution Composition			Membrane Description
	CA (g)	ZVI (g)	DMF Solvent (ml)	
CA	4.375	-	21.7	Neat CA
CA/ZVI-1	4.353	0.022	21.7	CA+ 0.5 wt% ZVI
CA/ZVI-2	4.310	0.065	21.7	CA+ 1.5 wt% ZVI
CA/ZVI-3	4.266	0.109	21.7	CA+ 2.5 wt% ZVI

Table 3. Permeability, thermal and roughness parameters of CA/ZVI MMMs

Membrane Type	Pure water Flux ($Lm^{-2}h^{-1}$)	Decomposition Temperature (T_d) °C	Weight loss (%)	Transition Temperature (T_g) °C	Average Roughness (nm)	R_{ms} Roughness (nm)
CA	15.61	248	97.5	191.2	16.15	21.55
CA/ZVI-1	37.17	284	71.58	201.5	31.83	49.16
CA/ZVI-2	25.63	304	48.23	216.2	58.31	76.51
CA/ZVI-3	13.43	316	34.27	218.4	95.32	123.65

Table 4. Effect of PEI binding on rejection performance of CA/ZVI-1 membrane.

Feed Sample	Rejection efficiency (%)					
	BOD (mg/L)		COD (mg/L)		SO_4^{2-} (mg/L)	
	CA	CA/ZVI-1	CA	CA/ZVI-1	CA	CA/ZVI-1
Raw textile dye effluent	77	95.8	68.6	88.5	1.46	15.5
PEI bound textile dye effluent	78.5	96.7	70.9	90.2	5.4	55.5

Table 5. Freundlich isothermal constants and R-squared fitting values for CA/ZVI-1 MMM

Rejection parameter	Without PEI binding			With PEI binding		
	R^2	m	b	R^2	m	b
BOD	0.9957	0.4989	0.0009	0.9852	0.3925	0.1202
COD	0.9948	0.4751	0.0112	0.9942	0.2839	0.1257
SO_4^{2-}	0.9998	2.799	0.0069	0.9903	1.834	0.0874

List of Figures

Fig.1.

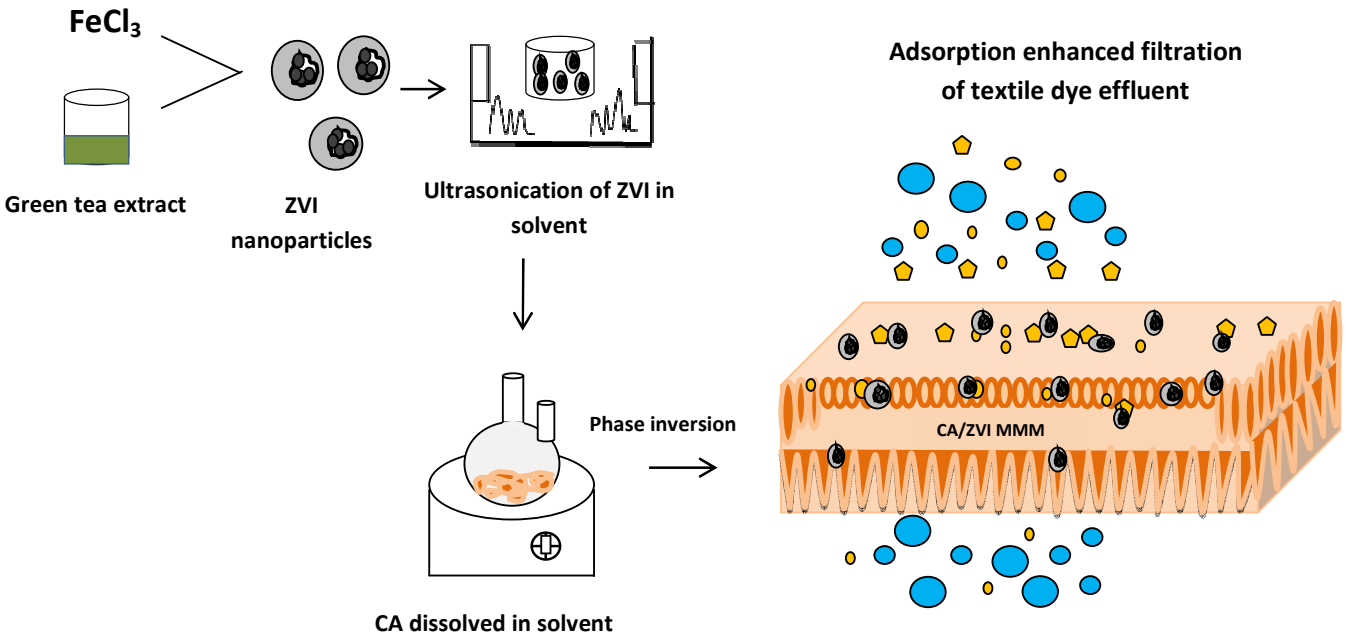

Fig.2.

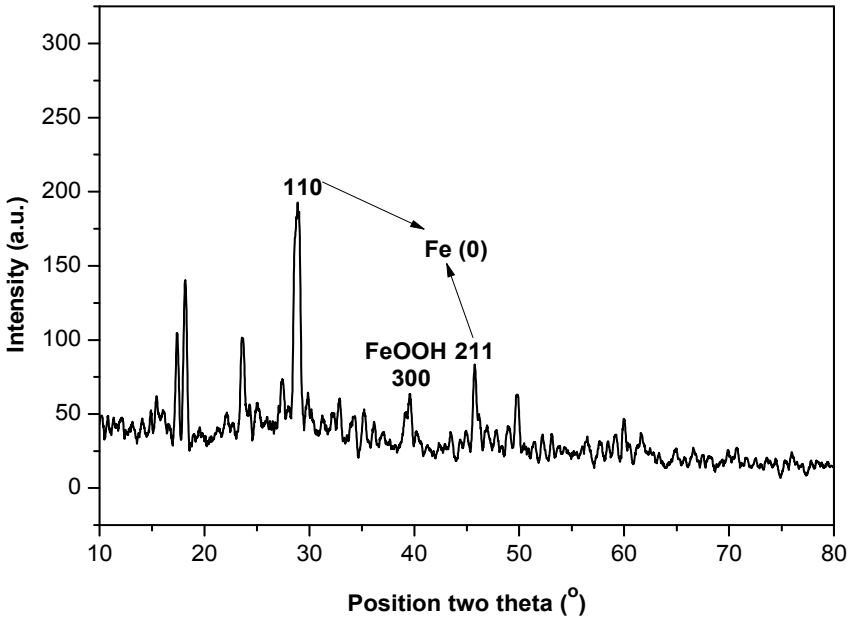

Fig. 3.

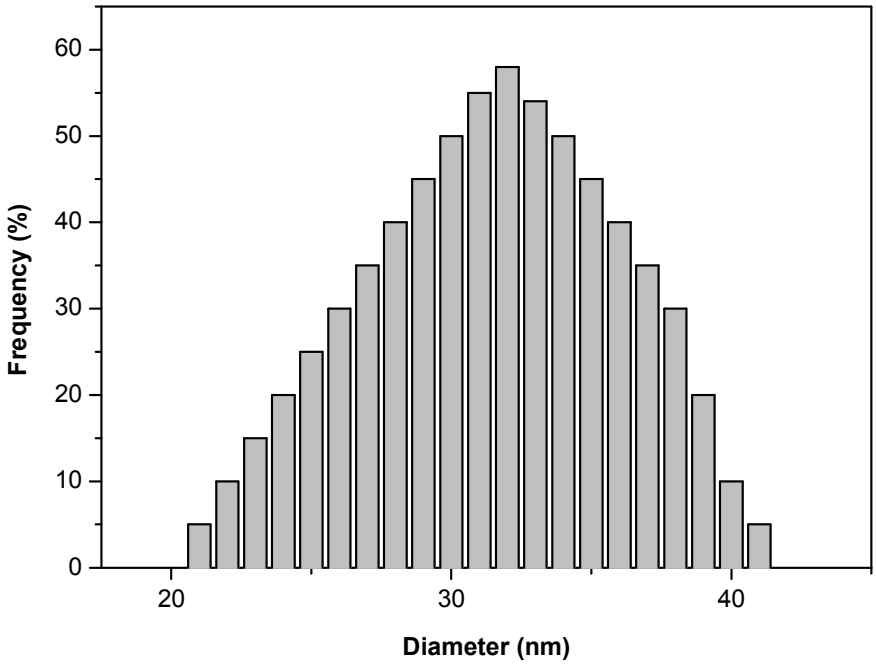

Fig. 4.

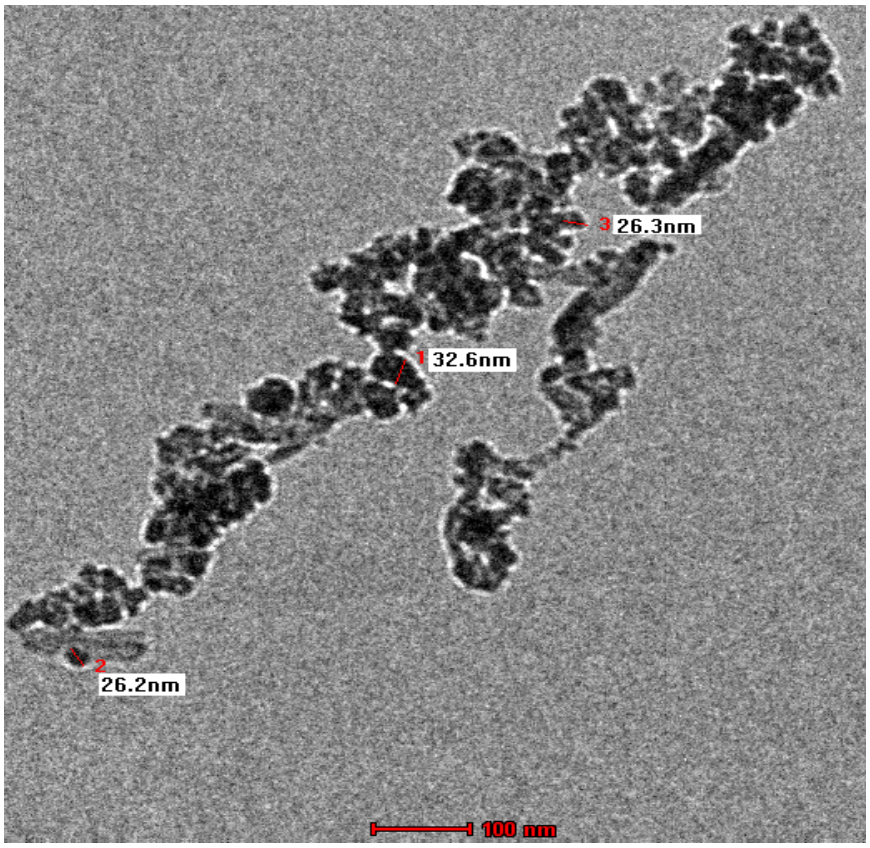

Fig. 5.

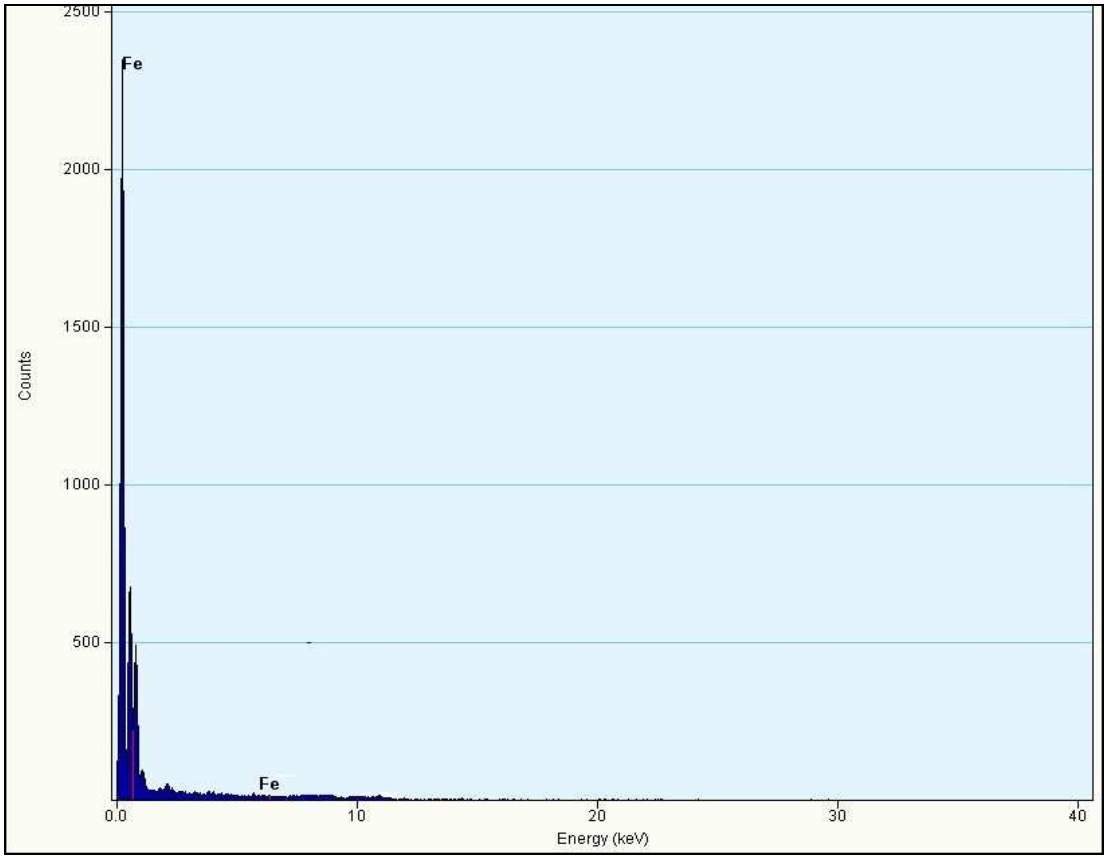

Fig. 6

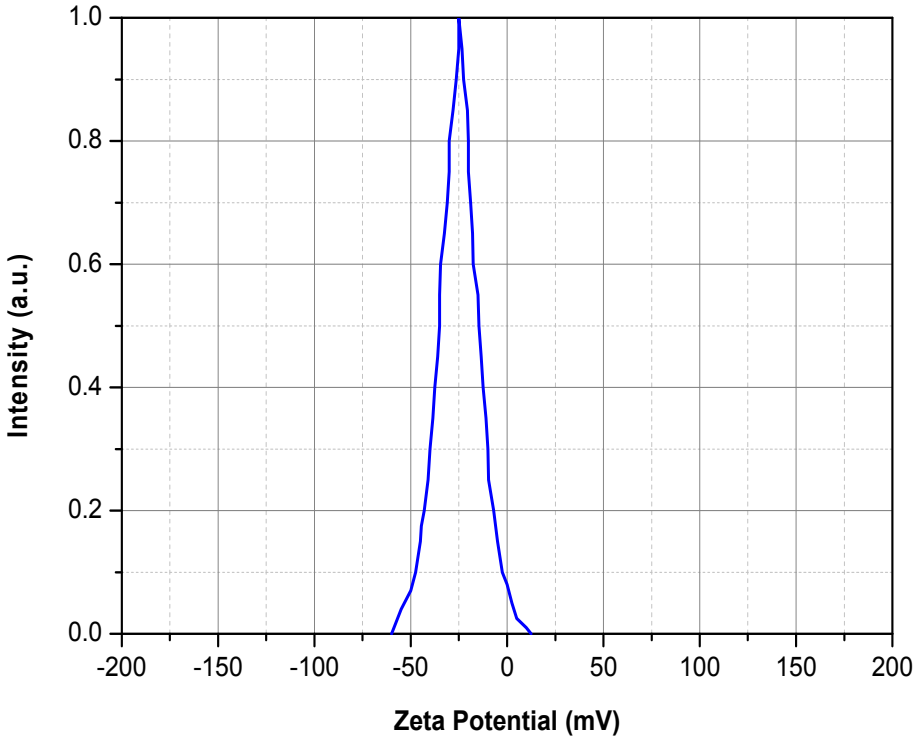

Fig. 7.

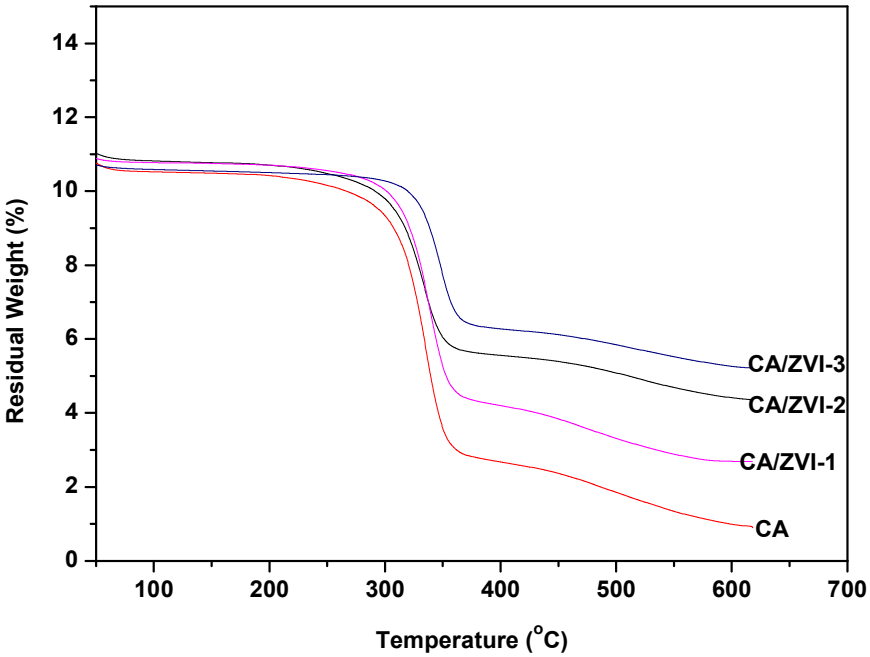

Fig. 8.

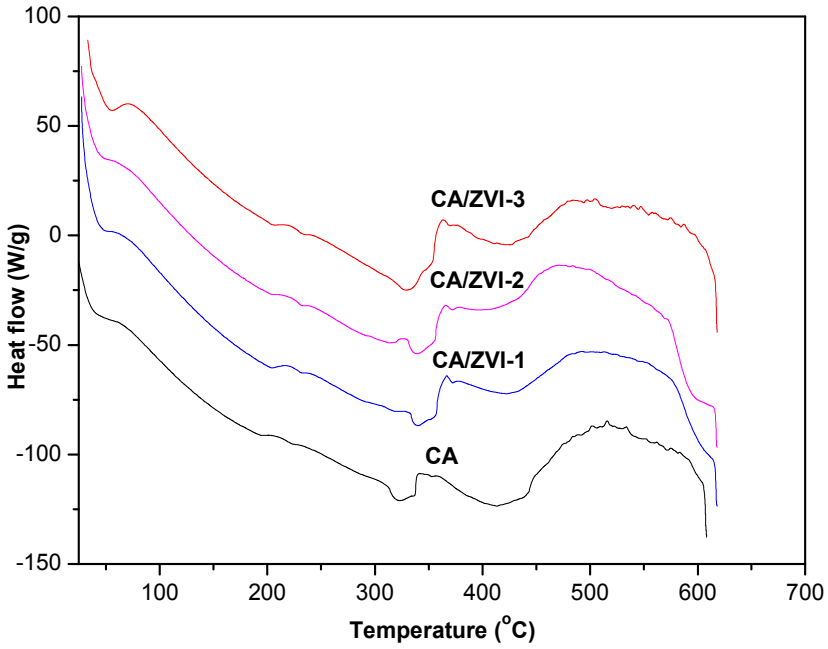

Fig. 9.

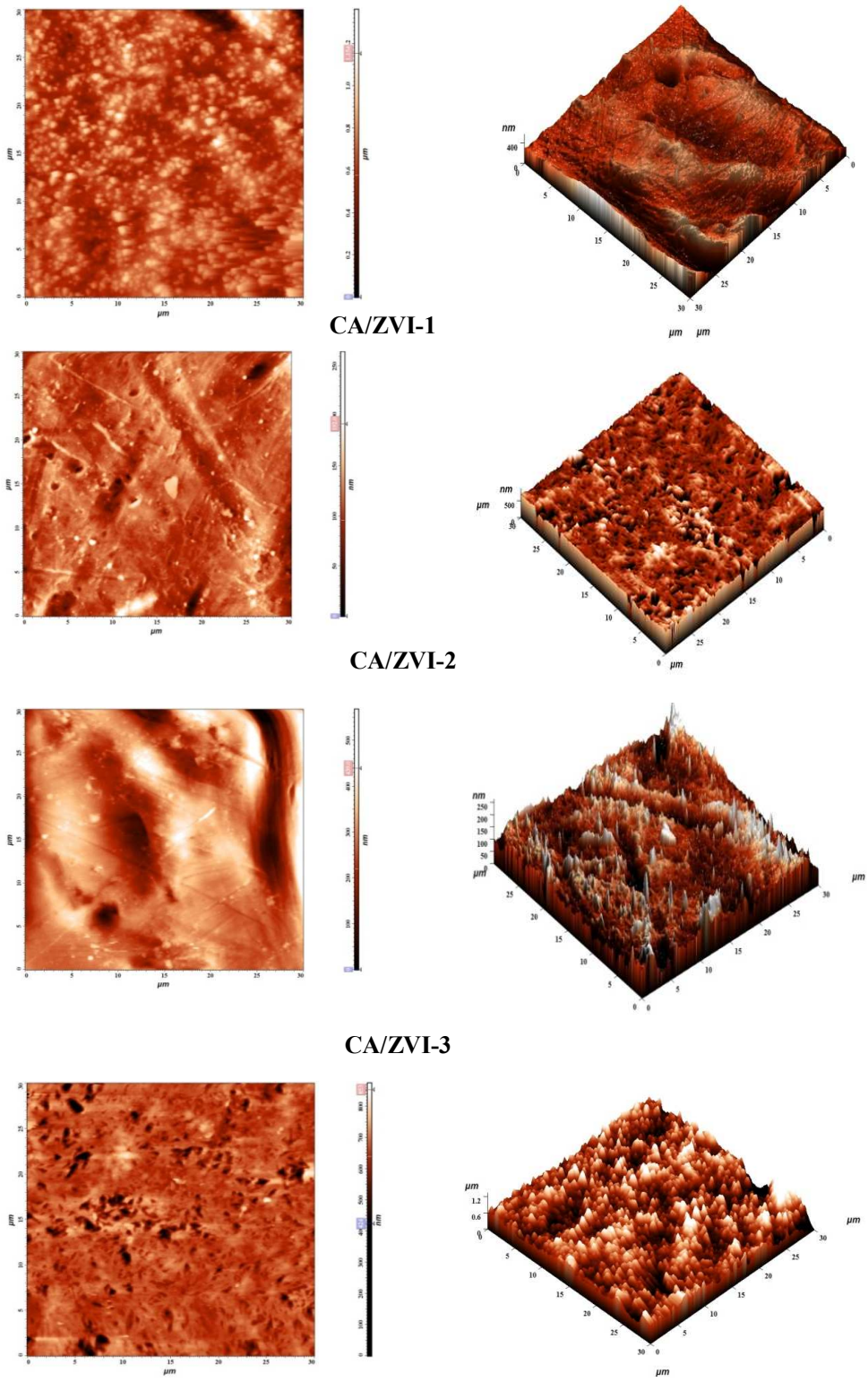

Fig. 10.

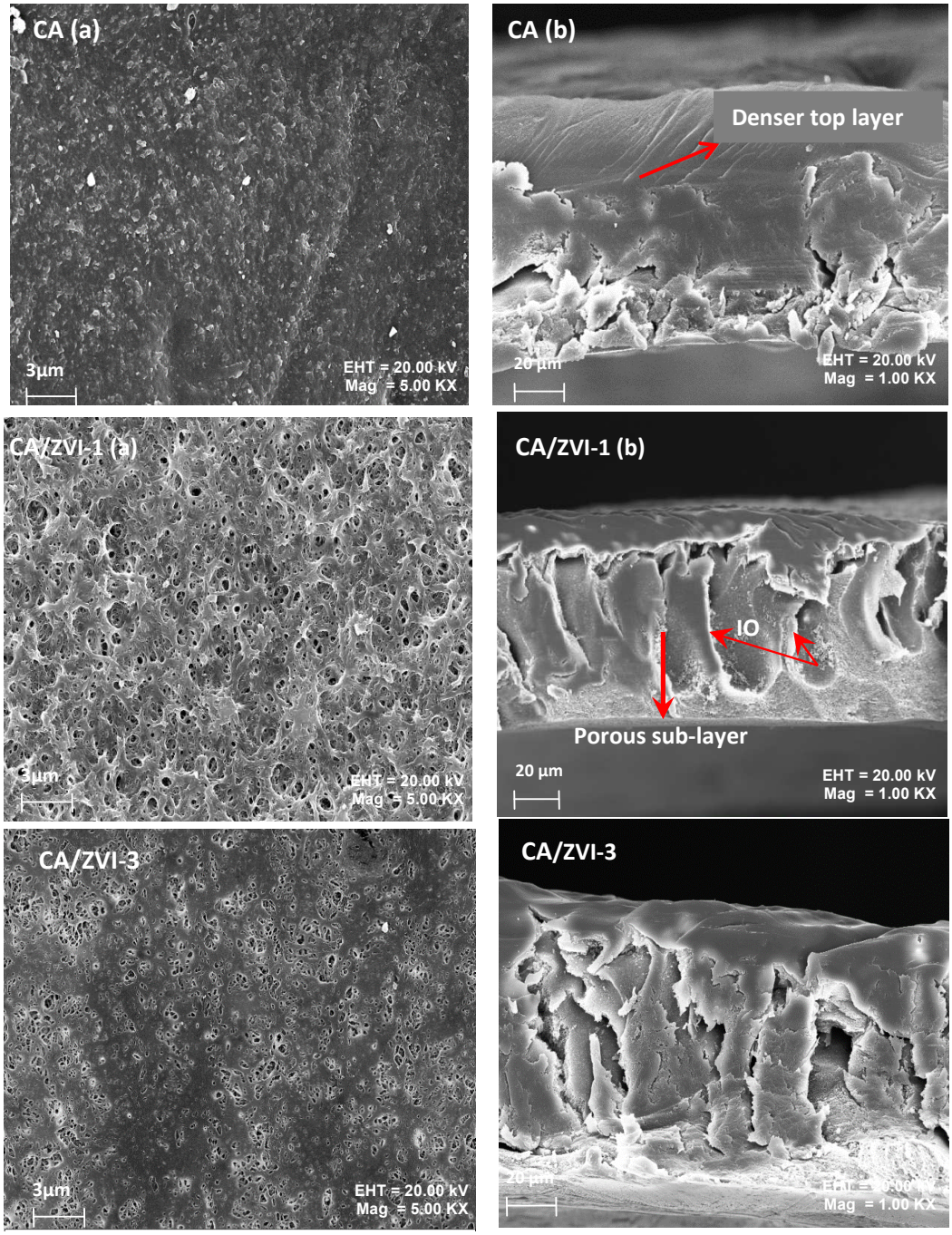

Fig. 11.

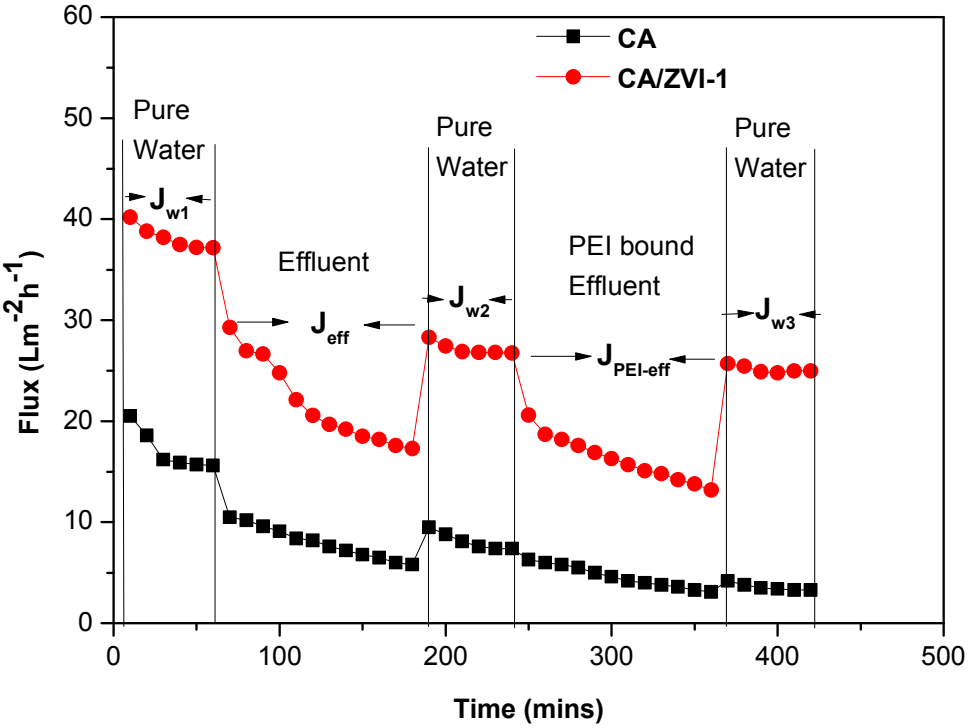

Fig. 12.

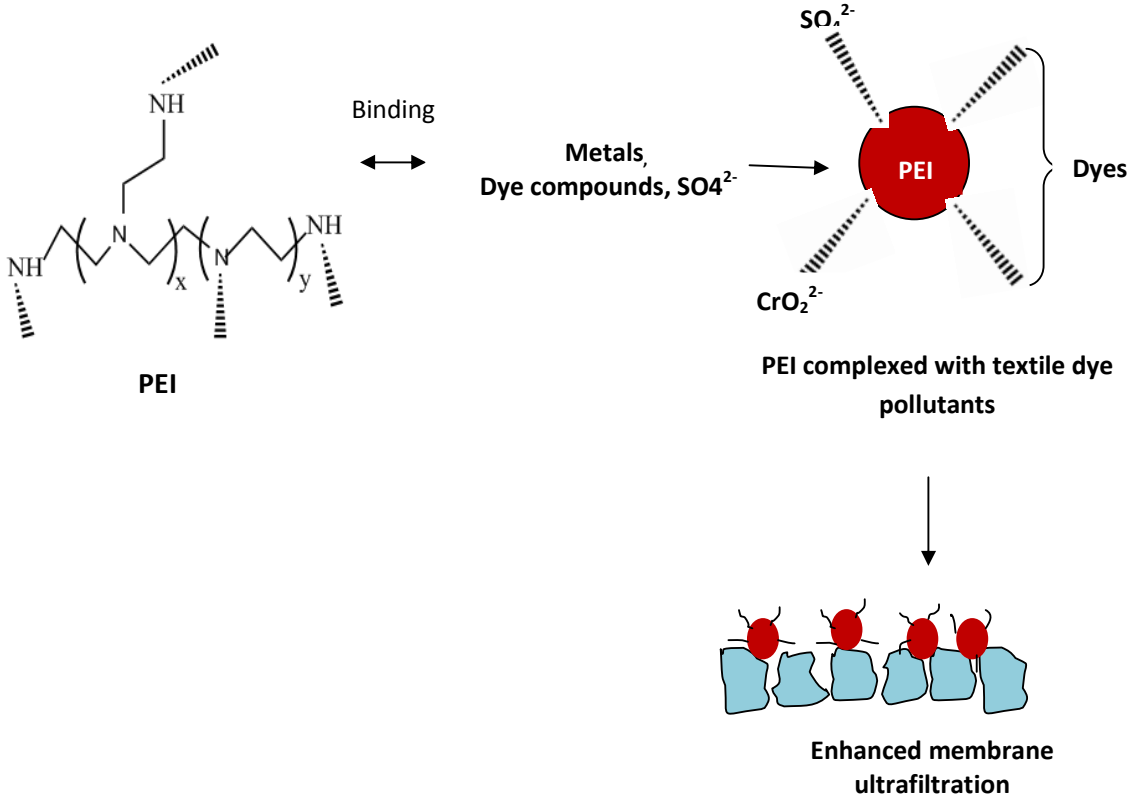

Fig. 13.

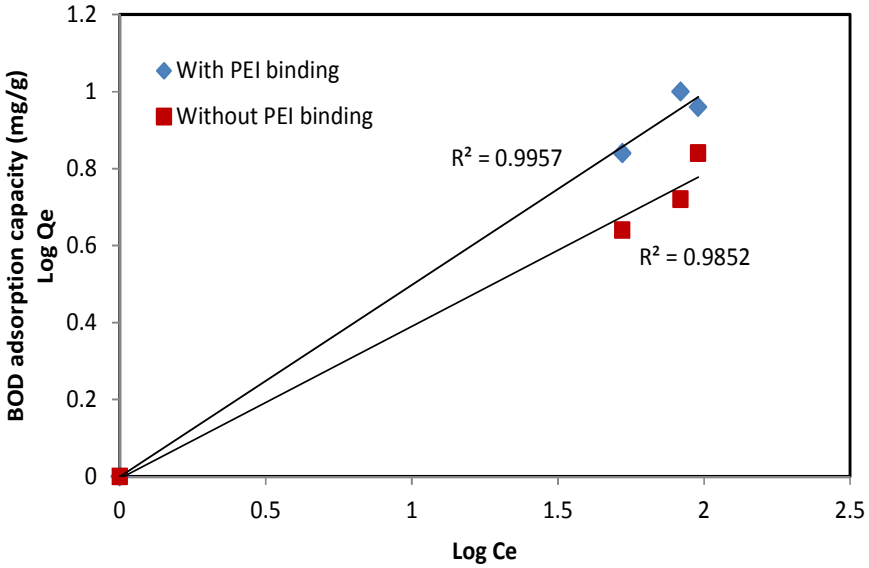

Fig. 14.

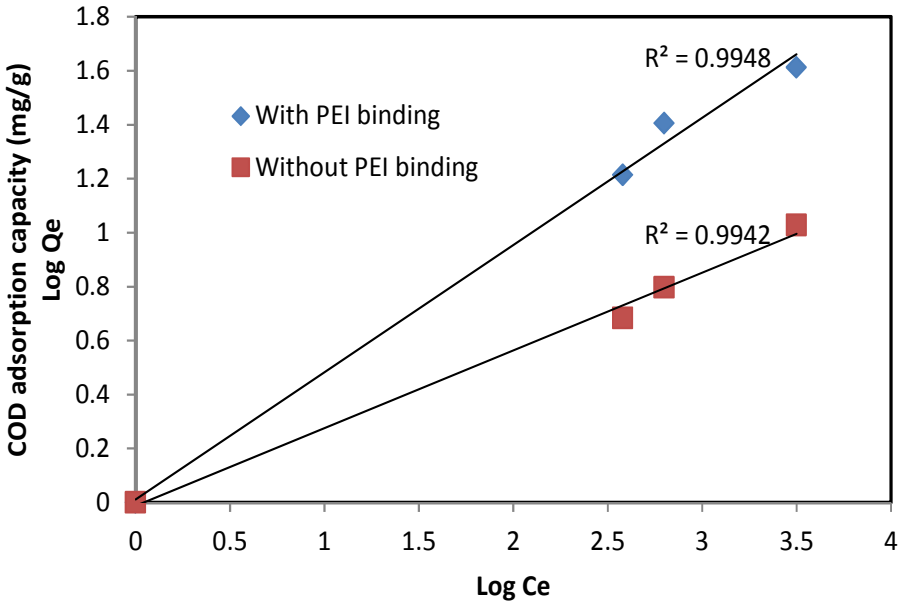

Fig. 15.